Magnetic susceptibility of YBa$_2$Cu$_3$O$_{6+x}$ crystals: Unusual Curie behavior and small contributions from charge density waves

I. Kokanović[1,2,*] and J. R. Cooper[1]

[1]*Cavendish Laboratory, University of Cambridge, Cambridge CB3 OHE, United Kingdom*
[2]*Department of Physics, Faculty of Science, University of Zagreb, P.O. Box 331, Zagreb, Croatia*

We report measurements of the magnetic susceptibility of twinned single crystals of YBa$_2$Cu$_3$O$_{6+x}$ from just above their superconducting transition temperatures to 300 K with magnetic fields of up to 5 T applied parallel and perpendicular to the CuO$_2$ planes at seven values of x. Appropriate analysis allows the relatively small, but still important, Curie terms to be separated from other contributions to the susceptibility. Our data support a picture in which the Curie terms arise from oxygen disorder in the Cu-O chains. This agrees with published work on polycrystalline samples where the sample cooling rate was varied, but here we show that the Curie plots flatten out above 200 K. We identify small effects of charge density wave (CDW) instabilities in the temperature (T) derivative of the in-plane susceptibility $d\chi_{ab}(T)/dT$ and discuss their x dependence. For $x = 0.67$ we make a detailed comparison with published high energy x-ray diffraction data using a minimal model involving Fermi arcs, thereby obtaining values for the CDW energy gap and the Helmholtz free energy in a coherence volume. At 80 and 100 K the latter is comparable with, or smaller than, $k_B T$, respectively, highlighting the probable importance of thermal fluctuations. We note that the effect of the Lorentz force on charge carriers in the Fermi arcs could provide a simple mechanism for enhancing the CDWs in high magnetic fields, as suggested by recent experiments.

I. INTRODUCTION

Nearly ten years ago the surprising observation of "slow" quantum oscillations in underdoped oxygen-ordered YBa$_2$Cu$_3$O$_{6.5}$ (YBCO) crystals [1] at high magnetic fields and then in the intrinsically underdoped stoichiometric compound YBa$_2$Cu$_4$O$_8$ [2,3], opened up new avenues in the study of high temperature superconductors. More recently, the presence of incommensurate charge density waves (CDWs) at temperatures (T) well above the superconducting transition temperature (T_c) has been established by a number of experiments, NMR [4], resonant x-ray scattering (RXS) [5–7], and high energy x-ray diffraction [8] both in YBa$_2$Cu$_3$O$_{6+x}$ and other underdoped cuprate superconductors [9–12]. It has been found that the wave vector of the CDW is directed along the copper-oxygen bonds and that it decreases slightly with increased hole doping [7,9,11–13]. Angle-resolved photoemission (ARPES) studies [9,14] of underdoped bismuth and lanthanum-based cuprates give evidence for Fermi arcs. In particular, Comin *et al.* [9] suggest that the CDW wave vector gives rise to small electron pockets [15] because it connects the tips of different Fermi arcs. This is appealing because it provides a direct link between the presence of the pseudogap and CDW formation. Namely the pseudogap is finite except in regions near the diagonals of the Brillouin zone (the nodal regions in the d-wave superconducting state). It therefore breaks the large Fermi surface, which has been observed directly via quantum oscillation studies of an overdoped cuprate [16], into disconnected arcs.

NMR measurements of underdoped YBCO give evidence for long-range static charge order in high fields, without any sign of spin order for $x > 0.5$ [17,18], while NMR measurements of quadrupolar frequency broadening suggest that the CDW order is also static at low fields [4]. Disorder may be important in low fields [19] and on the basis of earlier work on NbSe$_2$, it has been suggested that static CDWs nucleate around defects [4]. But somewhat against this, 2% Zn doping strongly suppresses the CDW intensity in YBa$_2$Cu$_3$O$_{6.6}$ [20]. Ultrasonic measurements at high fields [21] have also revealed a transition to a long-range charge ordered state, with further evidence being provided by two recent structural studies [22,23]. The ionic displacements associated with the CDW in UD67 YBCO ($T_c = 67$ K) have recently been calculated [24]. They reveal a complicated pattern involving shear displacements perpendicular to the CuO$_2$ layers that break the mirror symmetry of the bilayers. For this UD67 crystal Chang *et al.* [8] measured the intensity of CDW diffraction peaks as a function of temperature both at zero and finite magnetic fields. They observed a gradual increase in intensity below an onset temperature $T_{CDW} \simeq 135$ K and then, at zero field, a decrease below T_c. The behavior for $T < T_c$ suggested competition between the two types of order with the CDW signal being restored when superconductivity was suppressed by a large magnetic field. However, the origin of the CDW ordering vector, the driving force for CDW order, and the size of any CDW gap in the electronic density of states (DOS) are still unknown.

One fundamental thermodynamic property that could contribute towards understanding these questions is the T-dependent static magnetic susceptibility $\chi(T)$ above T_c. Here we report measurements of $\chi_c(T)$ and $\chi_{ab}(T)$ with magnetic field H parallel and perpendicular to the crystalline c axis for relatively large twinned single crystals of YBa$_2$Cu$_3$O$_{6+x}$ at seven values of the oxygen content x. In other CDW materials such as K$_{0.3}$MoO$_3$ [25] the opening of the CDW gap causes a clear reduction in $\chi(T)$, and an increase in $d\chi(T)/dT$ for $T \leqslant T_{CDW}$. Using a special method of analysis, which will also

*kivan@phy.hr

be useful in the future for studies of detwinned $YBa_2Cu_3O_{6+x}$ crystals and other underdoped cuprates, we show that for most, but not all, values of x, the onset of the CDW has a small but detectable effect on $d\chi_{ab}/dT$. From our viewpoint the physical reason for its small size is that as mentioned before [26] the electronic entropy at T_{CDW} has already been strongly suppressed because of the pseudogap. Or equivalently there are only short Fermi arcs rather than a large Fermi surface so the electronic DOS has already been heavily reduced by the pseudogap. In particular for our UD68 crystal with $T_c = 67.9$ K we compare our results with expectations from the T-dependent CDW intensity measured for UD67 [8], bearing in mind that the size of the CDW gap will be proportional to the square root of the intensity [27].

While performing this analysis we again found the surprising result, briefly mentioned previously [28], that the small isotropic Curie (C/T) terms in $\chi(T)$ disappear quite abruptly above 200 K. Since then, Biscaras *et al.* [29] have shown that fast cooling of polycrystalline $YBa_2Cu_3O_{6+x}$ from 400 to below 300 K, increases C and have suggested that Cu^{++} spins at the chain ends give a significant contribution to C, so that the longer chains in slowly cooled samples give a smaller Curie term. We discuss this picture and an alternative one in which the spins arise from localized states in the pseudogap [30]. Finally, using model parameters obtained by fitting our $d\chi_{ab}/dT$ data for UD68, we calculate the changes in electronic entropy, heat capacity, and the free energy density caused by the CDW. We discuss the importance of making high resolution heat capacity measurements of a detwinned UD67 crystal in the future, preferably combined with structural and magnetic susceptibility studies on exactly the same sample. From the present work we estimate the product of the free energy density and the CDW coherence volume in UD68 showing it to be $0.3k_BT$ at 100 K and $0.7k_BT$ at 80 K. These numbers are lower limits and could be 2 or 3 times larger if the effect of the pseudogap contribution is handled differently. Nevertheless it underlines the probable importance of thermal fluctuations that were previously mentioned in Ref. [4].

II. EXPERIMENTAL DETAILS

A $YBa_2Cu_3O_{6+x}$ crystal was grown by Iida [28] several years ago at the International Superconductivity Technology Center, Superconductivity Research Laboratory, Morioka, Iwate, Japan, using a modified crystal pulling method, often called the solute-rich, crystal-pulling method [31]. This method is unusual in that there is a layer of green phase Y_2BaCuO_5 at the bottom of the Y_2O_3 crucible below Ba-Cu-O liquid. In this situation, the liquid is always saturated with yttrium. Y_2BaCuO_5 is dense and always stays at the bottom of the crucible. In this work, as in Ref. [28], we measured pieces cut from a 1.5 g piece of this crystal. We have no independent estimates of possible inclusions of other phases in these pieces apart from our susceptibility data. Above about 150 K, possible inclusions such as Y_2BaCuO_5 [32] and $BaCuO_{2+x}$ [33] will give a Curie-Wiess term $\chi(T) \sim 0.375/(T + \theta)$ emu/mol with $\theta \sim 50$ and -70, respectively. For several values of x the Curie terms of our crystals were barely detectable. Taking the lowest value $C = 16 \pm 10 \times 10^{-4}$ emu K/mol, Table I, shows that there was at most 0.4 ± 0.25 mol % of these two

TABLE I. Summary of data. The first two columns show the final sample weights and the weight gain relative to the state with $x = 0.3$, giving the final values of x shown. The critical temperature T_c was taken from the onset of diamagnetism as determined by measuring field-warming magnetization at 10 Oe after zero-field cooling. C is the Curie constant and E_G/k_B is the pseudogap energy given by $1200[1 - (p/0.19)]$. The values of p are obtained from the $T_c(p)$ curve for annealed crystals in Ref. [35].

Weight (mg)	δm (mg)	x (meas)	T_c (K)	$10^4 C$ (emu-K/mol)	E_G/k_B (K)	p per CuO₂
85.83	1.05	0.81	84.9	33 ± 20	311	0.141
87.04	0.96	0.76	76.8	25 ± 10	353	0.134
85.62	0.84	0.71	71.9	16 ± 10	384	0.129
104.51	0.93	0.67	67.9	42 ± 20	413	0.125
254.13	2.01	0.63	64.0	84 ± 20	476	0.115
131.42	1.01	0.62	61.9	135 ± 20	512	0.109
234.13	1.12	0.50	57.0	50 ± 15	578	0.099

compounds. The level of possible inclusions of CuO can be estimated by comparing the peak in $d\chi/dT$ observed for CuO crystals [34] between 200 and 230 K with the noise level in our data, for example in Fig. 9. This gives a maximum of 2 mol % CuO. The value of T_c for an optimally doped piece of this crystal was 92.6 K [28], compared with 94.3 K in Ref. [35]. Strong in-plane scattering, for example from Zn/Cu substitution, suppresses T_c by ~ 13 K/at. % Zn [36], so in our crystals the number of strong in-plane scattering centers is at most 0.13 at.%.

Field-warming magnetization curves $M_c(T)$ at 10 Oe after zero-field cooling, shown later in the inset to Fig. 3, were extrapolated linearly to zero in order to define the critical temperature T_c. These values of T_c are listed in Table I. Samples are labeled by these T_c values rounded to the nearest integer, with prefixes UD denoting underdoped. The $M_c(T)$ data show sharp superconducting transitions with widths between the 50% and 90% points ranging from 0.6 to 1 K for all T_c values. $M_{ab}(T)$ curves measured in the same way gave the same values of T_c but their widths were a factor of 2 larger, probably because of the smaller values of the lower critical field H_{c1} parallel to the CuO_2 planes.

The values of x were determined more precisely than in our previous paper [28]. Two separate pieces of the as-grown crystals, weighing 55 and 111 mg were annealed in flowing argon for 12 h at 750 °C, and their weight loss measured to 0.01 mg. A second identical anneal gave no further weight loss. This procedure gave $x = 0.300 \pm 0.004$, which is consistent with the observation that the samples were barely superconducting together with the $T_c(x)$ curve shown in Fig. 1(c) [35]. Pieces of the as-grown crystal were then annealed under different conditions [38] to give the seven samples UD85 through to UD57 with the values of x being obtained from the weight changes summarized in Table I. In the present work crystals were mounted and cooled in the SQUID magnetometer after being stored for 1 to 30 months at room temperature [38]. This is in contrast to our earlier study [28], where SQUID measurements for the samples in Fig. 1 of Ref. [28], but not the other crystals in that paper, were made 1 to 2 h after quenching the crystal on to a copper block. The
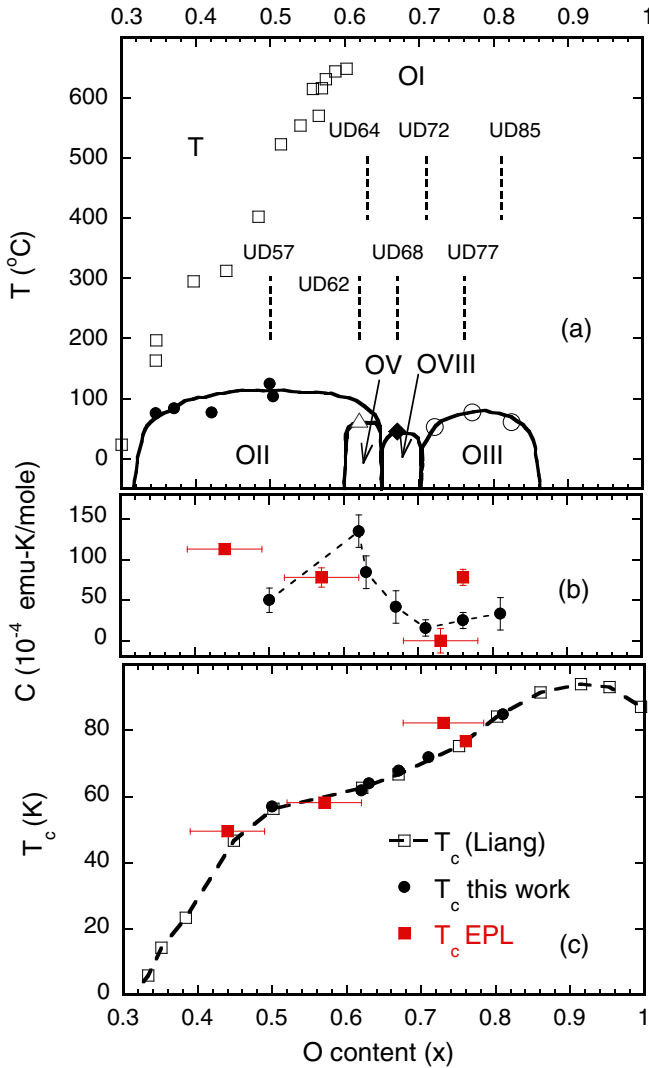
FIG. 1. (a) Oxygen ordering diagram adapted from Ref. [37] showing the various ordered states of the Cu-O chains and the crystals studied here. (b) Curie terms for the samples reported here (black circles). (c) Comparison of T_c versus oxygen content x in the present YBa₂Cu₃O$_{6+x}$ crystals after long annealing times between 20 and 25 °C (black circles) with data for detwinned and annealed crystals from Ref. [35], open squares. In (b) and (c) data for annealing times of 1 to 2 h from Ref. [28] (red squares larger error bars) and for UD77 after 24 h are also shown.

oxygen contents of the crystals reported here are represented by dashed lines on the oxygen ordering diagram in Fig. 1(a) which is adapted from Ref. [37]. However, we have no direct proof that this phase diagram applies to our crystals. They have been annealed at room temperature for extremely long periods, during which weight changes were less than 0.01 mg, but they were not detwinned. This weight change limit corresponds to an uncertainty in x ranging from 0.002 for a 234 mg crystal to 0.005 for an 83 mg one. Because of this twinning it is important to note that as shown in Fig. 1(c), $T_c(x)$ agrees with that of the crystals used for the CDW studies mentioned in the Introduction. For the CDW studies the various ordered phases OV, OVIII, etc. shown in Fig. 1(a) were achieved using special

annealing procedures applied to de-twinned crystals [39]. However, for some values of x quantum oscillations were only observed for YBCO crystals where the OV and OVIII order had been suppressed by quenching from 100 °C [40] because surprisingly, at least for OVIII, this increases the carrier mean free path [41]. Furthermore, structural studies on rapidly quenched crystals still show CDW effects although their amplitude is reduced [42]. The annealing procedures should lead to longer Cu-O chains, an increase in p [35] and smaller Curie terms [29].

Figure 1(b) shows the Curie constants C for the present crystals together with three quenched crystals from Ref. [28]. The latter have larger uncertainties in x which hampers detailed comparison. We can only say that the values of C are similar. One further sample, UD77, for which OIII order could be expected, was measured one day after quenching and again 30 months later. There was no detectable change in T_c but a substantial fall in C, as also shown in Fig. 1(b). An important caveat is raised later, but if we do make the simple assumption [29] that each chain end gives rise to one spin $s = 1/2$, and assume that a localized spin always separates two chain segments, then the number of spins is equal to the number of chain segments. Hence the values of C in Fig. 1(b) and Table I ranging from 135 to 16 × 10^{-4} emu K/mol and corresponding to 0.036 to 0.0043 $s = 1/2$ spins per unit cell, give average chain segments ranging from 11 to 88 nm. These are 2 to 15 times larger than CDW coherence lengths [7].

Optical microscope images of the twin patterns in our UD57, UD62, UD64, and UD68 crystals showed typical spacings of 1000 nm corresponding to a limit of 1400 nm on the chain lengths from this source. The UD64 and UD68 crystals appeared to be completely twinned but for UD57 and UD62, twins could only be seen in about 50% of the area studied. For UD68 there were clear microcracks separated by ≃50 μm which aided oxygenation. From the above arguments it is probable that the twinning described here does not have significant effects on the CDW. However, against this, it is considered that twinning causes stress and macroscopic oxygen segregation in YBCO crystals [39]. So similar measurements and analysis of detwinned YBa₂Cu₃O$_{6+x}$ crystals would be worthwhile if sufficiently large (50 mg or more) and uniformly oxygenated crystals can be obtained.

III. RESULTS AND ANALYSIS

The temperature dependencies of the static magnetic susceptibility $\chi_c(T)$ ∥ to the c axis and $\chi_{ab}(T)$ ∥ to the ab plane for $H = 5$ T are shown in Fig. 2, while Fig. 3 shows the susceptibility anisotropy, defined here as $\chi_D(T) = \chi_c(T) - \chi_{ab}(T)$, for the seven YBa₂Cu₃O$_{6+x}$ crystals studied. It can be seen in Figs. 2 and 3 that above 200 K $\chi(T)$ increases with T for all samples, which we ascribe to the pseudogap having a substantially larger value than any possible CDW gap, in line with arguments put forward in Refs. [4,26,43]. For UD64 and UD62 there are upturns below 150 K that are clearly visible in $\chi_{ab}(T)$ in Fig. 2 but are absent in the corresponding $\chi_c(T) - \chi_{ab}(T)$ data in Fig. 3. This strongly suggests that there is an isotropic Curie term as found previously [28].
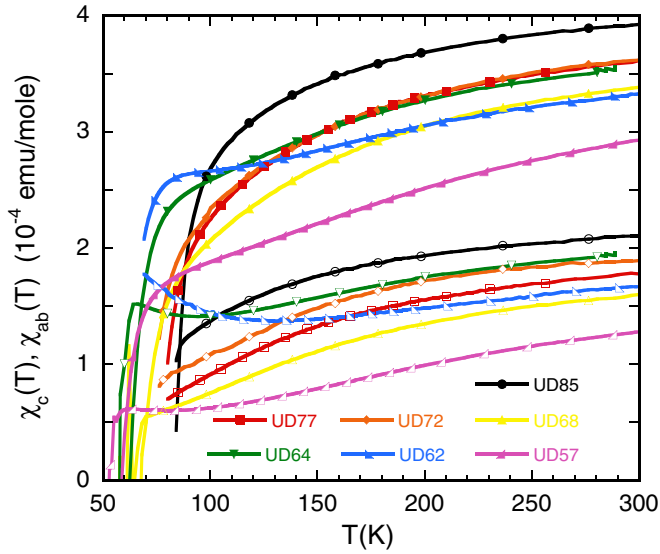
FIG. 2. Temperature dependence of the static magnetic susceptibility $\chi_c(T)$ (full symbols) and $\chi_{ab}(T)$ (empty symbols) for $H = 5$ T $\parallel$ the c axis and the ab plane, respectively.

A. Analysis of Curie terms

Figure 4(a) shows plots of $\chi_c(T)$ vs $\chi_{ab}(T)$ for all samples studied with T as an implicit parameter. This method of analysis was originally applied to $Bi_2Sr_2CaCu_2O_{8+\delta}$ crystals [44]. With the notable exceptions of UD64 and UD62 they are linear with a slope of 1.4 over an extended range before turning down because of the diamagnetic superconducting fluctuation term which is predominantly in $\chi_c(T)$ because of the large anisotropy [45]. This downturn sets in quite abruptly somewhat below $\simeq 130$ K. Therefore, in Fig. 5 we plot $1.4\chi_{ab}(T) - \chi_c(T)$ vs $1/T$ down to 125 K. Such a plot
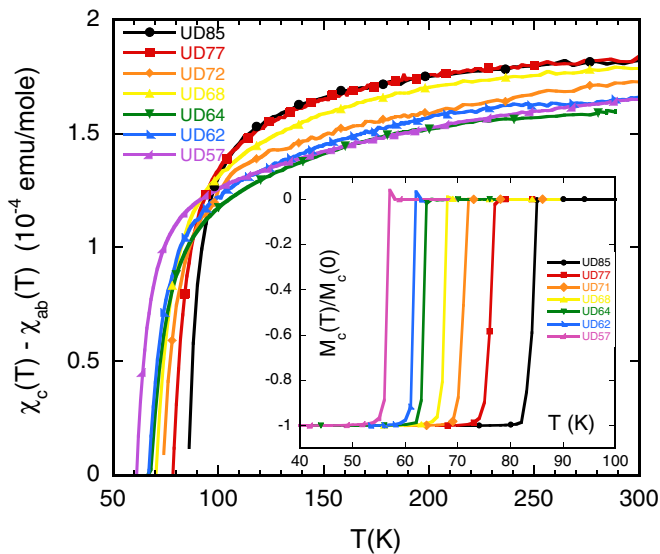

FIG. 3. Susceptibility anisotropy $\chi_D(T) = \chi_c(T) - \chi_{ab}(T)$ for $YBa_2Cu_3O_{6+x}$ single crystals. Inset: Superconducting transitions of the $YBa_2Cu_3O_{6+x}$ crystals for $H\parallel c$ measured on warming in 10 G after zero-field cooling.
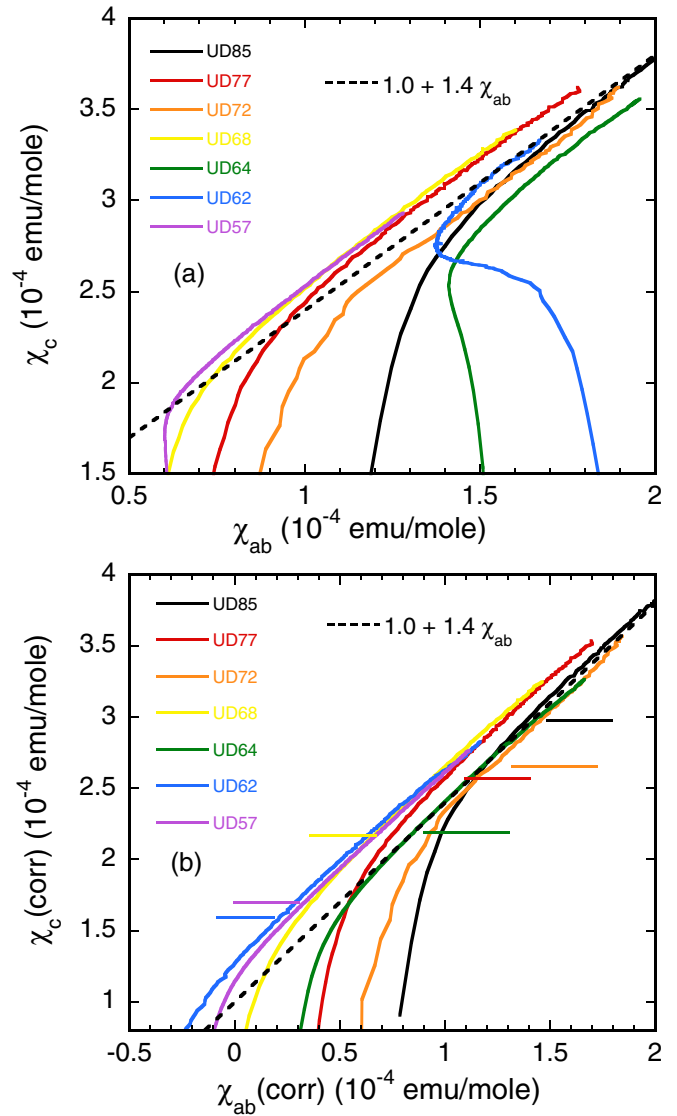

FIG. 4. Plots of static magnetic susceptibility $\chi_c(T)$ with $H \parallel$ the c axis versus $\chi_{ab}(T)$ with $H \parallel$ to the ab plane (a) for the data shown in Fig. 2 and (b) after subtracting the Curie terms shown in Fig. 1(b) and Table I. The dashed line shows the behavior expected for a constant anisotropic g factor with $(g_c/g_{ab})^2 = 1.4$ [28], the color-coded horizontal lines show $\chi_c(130)$.

eliminates any susceptibility contributions arising from the pseudogap as discussed previously [28] and from any CDW under the reasonable assumption that it also has a g^2 anisotropy of 1.4 as suggested by the dashed line in Fig. 4(a). It therefore allows the isotropic Curie term to be identified. The linear regions in Fig. 5 between 200 and 130 K give the Curie constants for each crystal. When they are subtracted from both $\chi_c(T)$ and $\chi_{ab}(T)$ the corrected plots are then linear down to at least 130 K as shown in Fig. 4(b) where the values of $\chi_c(130)$ are marked by horizontal lines. A surprising result in Fig. 5 is that the Curie plots for all crystals flatten off and deviate from $1/T$ behavior above 200 K. The inset to Fig. 5 shows Curie plots obtained by scanning in data from Figs. 1 and 3 of Biscaras *et al.* [29] and converting them to the units used here. These refer to experiments in which the
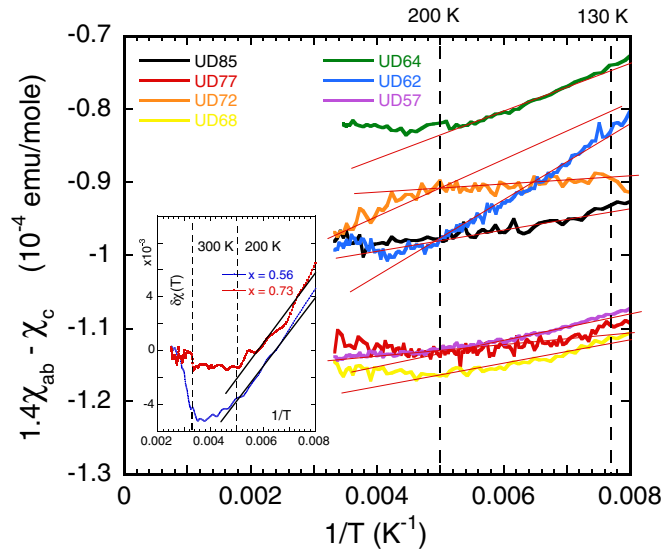
FIG. 5. Plots of $1.4\chi_{ab}(T) - \chi_c(T)$ vs $1/T$ for the long-time annealed crystals studied here. The linear regions between 200 and 130 K are used to determine the Curie terms C for each sample, shown in Fig. 1(b) and in the inset to Fig. 6. Errors in C were obtained by making similar plots (not shown) for $(g_c/g_{ab})^2 = 1.35$ and 1.45. The inset shows data from Ref. [29] where $\delta\chi(T)$ (converted to the units used here) is the difference between fast and slowly cooled polycrystalline samples of YBCO with the x values shown. In all cases, except UD72 (see text), the Curie term tends to go away above 200 K.

FIG. 6. In-plane magnetic susceptibility $\chi_{ab}(T) - C/T$ of the seven YBa$_2$Cu$_3$O$_{6+x}$ samples studied after subtraction of the Curie terms C/T obtained using the procedure given in the text. For UD68 the measured values of $\chi_{ab}(T)$ are also shown. The inset shows the dependence of three quantities on oxygen content x: the average susceptibility $\chi_{av} \equiv \frac{2}{3}\chi_{ab} + \frac{1}{3}\chi_c$ at 200 K (blue squares) after subtracting the Curie terms, published data for polycrystalline YBa$_2$Cu$_3$O$_{6+x}$ [46], black circles, where no Curie term has been subtracted, and the Curie term C itself in units of 10^{-4} emu K/mol. $C = 37.5 \times 10^{-4}$ emu K/mol corresponds to 0.01 spin-$\frac{1}{2}$ centers per formula unit.

same polycrystalline samples of YBa$_2$Cu$_3$O$_{6+x}$ were measured using a SQUID magnetometer in both the rapidly cooled (10 K/min) and slowly cooled (1 K/min) states. Fast cooling gives less order in the Cu-O chains below 300 K and hence slightly larger Curie terms that are visible in the difference plots shown. The data for $x = 0.73$ shown in the inset to Fig. 5 are particularly clear because there are large deviations from a Curie law above 200 K but only minor changes at higher T. This strongly supports our finding that the Curie plots flatten off above 200 K. However, the magnitudes of the Curie terms obtained from the main part of Fig. 5, that are tabulated in Table I, are typically a factor of 10 larger than the value for difference plots, $C = 2.7 \times 10^{-4}$ emu K/mol shown by the straight lines in the insert to Fig. 5.

Because all our samples are derived from the same large crystal, we can confirm the result of Ref. [29] that the Curie terms are caused by oxygen disorder in the chains and therefore faster cooling increases C by $\sim$10%. The results in Fig. 1(b) suggest that this disorder could be particularly large for OV crystals and that for OIII ones long annealing times at room temperature increases the chain order. However, we feel that further evidence such as ESR or NMR data is needed in order to be sure that the C/T terms are indeed caused by Cu^{++} ions in the chains. For Zn doped La$_{2-x}$Sr$_x$Cu$_{1-y}$Zn$_y$O$_4$ samples it was found that Zn substitution introduced Curie-like behavior [30]. In this case it was argued [30] that disorder induces a transfer of spectral weight from the wings of the pseudogap to low energies. It is possible that oxygen disorder in the Cu-O chains of YBCO is having the same effect. Some support for this picture is given by Curie plots (not shown
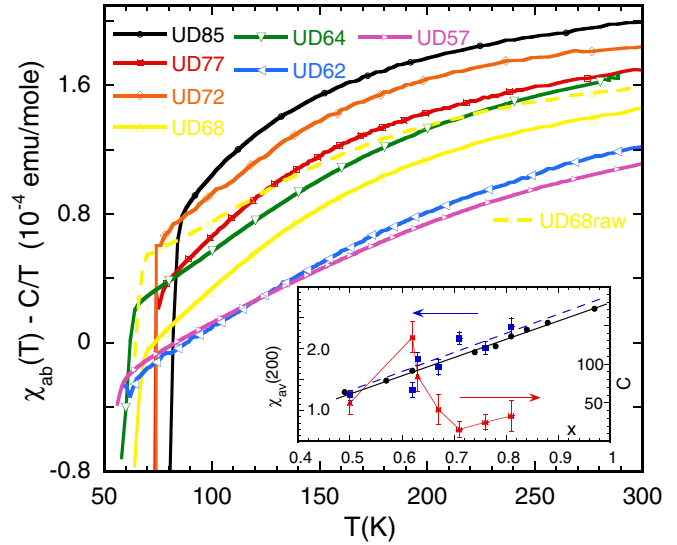
here) of the difference data in Ref. [29]. For x values ranging from 0.79 to 0.43, but not for lower values, departures from C/T behavior occur at gradually increasing temperatures as x decreases, i.e., as the pseudogap gets larger.

If either scenario involving oxygen disorder in the chains is adopted then the flattening out above 200 K could be connected with evidence from thermal expansion studies [47] for time-dependent "glassy" behavior down to 230 K for YBa$_2$Cu$_3$O$_{6.95}$. This is absent for YBa$_2$Cu$_3$O$_{7.0}$ where the Cu-O chains are all full. The abrupt change in $\delta\chi$ above 300 K for $x = 0.56$ shown in the inset to Fig. 5 is caused by a decrease in p when the slowly cooled sample is heated above 300 K. At this point the Cu-O chains in slowly cooled samples become less ordered and p falls slightly, as noted previously [48] in work on the electrical resistivity and the Hall effect of epitaxial YBCO films. Figure 6 shows the values of $\chi_{ab}(T)$ for the seven YBa$_2$Cu$_3$O$_{6+x}$ samples studied, after correction for the Curie terms. These do not have any contributions from localized spins or from superconducting fluctuations [45] (except possibly a few K above T_c) and can therefore be examined for the possible influence of CDWs. It is clear that $\chi_{ab}(T)$ is continuing to rise at 300 K, which we ascribe to a separate effect from the pseudogap in agreement with several other research groups [4,26,43]. Apart from the T dependence caused by the pseudogap, there is no obvious sign of CDW effects with an onset temperature $T_{\text{CDW}} \simeq 150$ K found in the NMR [4] and structural [6–8,13] studies cited in the Introduction. We therefore take a closer look at $d\chi_{ab}(T)/dT$ in the following section. The T-dependent

curves in Fig. 6 would be appropriate for comparison with local probes of the spin susceptibility such as Y^{89} Knight shifts [49] or Gd^{3+} electron spin resonance shifts [50], although the region above 200 K should be handled with care because in Fig. 6 we have subtracted the C/T Curie correction term over the full range of T even though we think that the localized spins become delocalized above 200 K. The variation of these curves with oxygen content x is reasonably smooth and monotonic after including possible measurement errors and the errors in C. This is illustrated in the inset to Fig. 6 where the average susceptibility $\chi_{av} \equiv \frac{2}{3}\chi_{ab} + \frac{1}{3}\chi_c$ at 200 K (where we can be more confident of the Curie term C and are still well above the superconducting fluctuation region) is compared with the smoother variation obtained for polycrystalline samples [46]. After including conservative measurement errors (corresponding to the absence or presence of 2 mm of the plastic tube holding the sample) and the errors in C, the data for all samples except UD62 are reasonably consistent with the blue trend line for crystals and the black line for polycrystalline samples shown in the inset. The blue line is drawn slightly higher than the black one because a small amount of preferential alignment in our polycrystalline samples reduced χ_{av} slightly [28]. We note that the extrapolated intercepts in Fig. 5 at $1/T = 0$ have a spread of 0.3×10^{-4} emu/mol. If this is converted into a standard deviation (σ) in χ_c and χ_{ab} (taken to be the same) it gives $\sigma = 10^{-5}$ emu/mol, consistent with the scatter and the error bars in the inset to Fig. 6 and with the level of nonmonotonic behavior with x that can be seen in the main part of this figure. The exception to the above discussion is UD62 for which C is $135 \pm 20 \times 10^{-4}$ or $85 \pm 25 \times 10^{-4}$ emu K/mol larger than that for UD58. In Ref. [29] it was argued that for $x = 0.45$ one spin-1/2 center per unit cell decreases the planar hole concentration by 0.5 per unit cell. Applying the same model to UD62 reduces its p value to 0.103 ± 0.002 (relative to UD58) which is very close to that for UD58, in line with their values of $\chi_{ab}(T) - C/T$ and $\chi_{av}(200)$ in the main part of Fig. 6 and the inset, respectively. In summary, from the discussion in this section we conclude that the Curie term in our samples is important for detailed understanding and that it is reasonably well understood at an empirical level.

B. Possible effects of CDWs on derivative plots

Figure 7 shows derivative plots $d\chi_{ab}(T)/dT$ vs T for the seven long-time annealed crystals studied here on the same scales, with a view to detecting the onsets of CDW order in the temperature ranges given by RXS [7]. Raw derivatives (not shown) were obtained by subtracting neighboring $\chi_{ab}(T)$ points and dividing by the 1 to 4 K difference in their T values. They were then smoothed using a sliding average of 5 points. We have also calculated the derivatives from the raw data using sliding second order polynomial fits to groups of 3, 5, or 7 adjacent points. These give the same results with no significant differences for different smoothing ranges. The orange curves show the derivatives after smoothing while the black curves include the C/T^2 correction for the Curie term. Note that this has been added for all T even though Fig. 5 shows clear deviations from a Curie law above 200 K. For several values of x, C is small so there is little difference
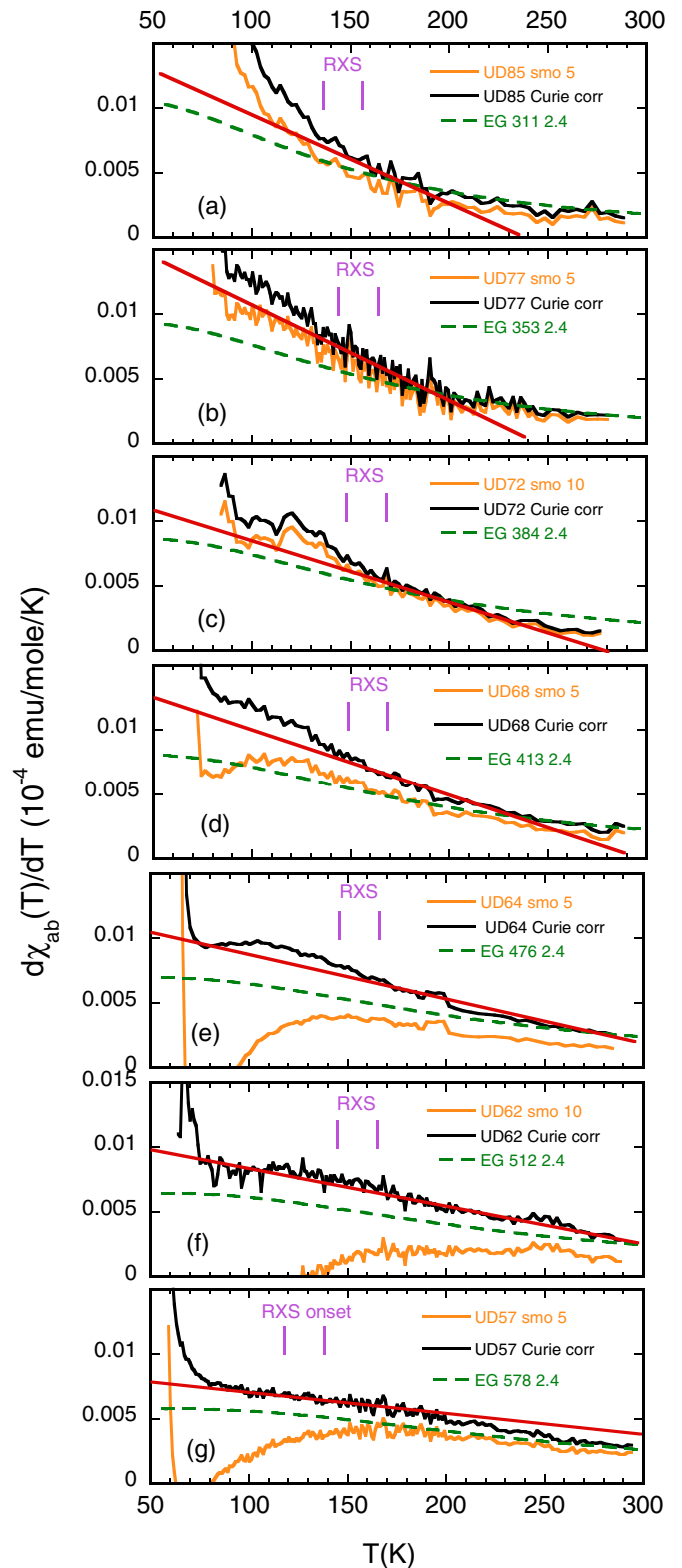

FIG. 7. Smoothed derivative plots $d\chi_{ab}(T)/dT$ vs T for all crystals studied here, orange lines. Solid black lines show the effect of adding C/T^2 which removes the Curie term arising from localized spins. The red lines and the green dashed lines show different ways of defining the background signal caused by the pseudogap (see text). The T_{CDW} onset temperatures, including their errors bars, obtained from resonant x-ray scattering for each value of x [7] are shown by the vertical purple lines.

between the orange and black curves. For the samples where C is larger, there is no obvious transition between the black and orange curves above 200 K. We believe the flattening of the Curie plots above 200 K is largely compensated either by a small increase in p above 200 K, in the "Cu^{++} chain scenario," or by an effective reduction of the pseudogap energy in the "low energy spectral weight" picture.

In order to see the effect of the CDWs we have to define a T-dependent background caused by the pseudogap. In view of the flattening of the Curie plots above 200 K we have defined our "best" background as a straight line that fits the data from the onset $T_{CDW} \sim 150$ K given by RXS up to 200 K. These straight lines are shown in red in Fig. 7. An alternative way of determining the background contribution to $d\chi_{ab}(T)/dT$ is to use Loram's triangular gap model for the DOS. This is a first-order phenomenological model, describing a nodal pseudogap that accounts for a large body of heat capacity (entropy) and magnetic susceptibility data [51] for polycrystalline cuprates and some magnetic susceptibility data for single crystals [28]. It gives

$$\chi_{PG}(T) = A\{1 - y^{-1}\ln[\cosh y]\}, \quad (1)$$

where $A = N_0(g\mu_B)^2$, $y = E_G/2k_BT$, N_0 is the electronic DOS at high energies, assumed to be independent of energy, and E_G is the pseudogap energy. Previously [28] we took $A = 3.0$ and 4.2×10^{-4} emu/mol for χ_{ab} and χ_c corresponding to an average spin susceptibility at high T of 3.4×10^{-4} emu/mol. This model does not include Fermi arcs which according to Ref. [52] are "protected" regions that are responsible for superconductivity in underdoped cuprates. The length of these arcs can be estimated from the ratio of the superfluid densities (squares of the London penetration depths) at low T for YBa$_2$Cu$_3$O$_7$ and YBa$_2$Cu$_3$O$_{6.5}$ [53]. In a minimal model with an underlying cylindrical Fermi surface the arcs are $\simeq 20\%$ of the circumference.

Provided the pseudogap energy increases linearly from zero at the tips of the arcs towards the antinodes, the triangular gap model will still apply but with A values reduced by a factor 0.8 and with an additional T-independent paramagnetic contribution of $0.2A$, which will not show up in the derivative. The green dashed lines in Fig. 7 show calculated $d\chi_{ab}(T)/dT$ vs T curves obtained from Eq. (1) with these reduced values of A and E_G/k_B given by $1200[1 - (p/0.19)]$ [51], with values of p given in Table I that were determined from the $T_c(p)$ relation of Liang *et al.* [35].

With the exception of UD72 (which may be atypical in that there appears to be a Curie term above 200 K in Fig. 5 and none below) and UD62 which has a relatively large Curie term, the green curves give reasonably good fits to the data in Fig. 7, but as shown later for UD68 on an expanded y scale in Fig. 9 they are not as good as a linear background. They also tend to give T_{CDW} values that are somewhat higher than RXS, but this would be consistent with Raman studies where $T_{CDW} \simeq 175$–200 K [54]. For the green curves, CDW effects in the derivative plots near 100 K are up to a factor of 2 larger than when using the red lines as background. However, we note that taking $A = 2.4 \times 10^{-4}$ emu/mol is based on the assumption of a cylindrical Fermi surface. Band-structure calculations usually give a larger DOS in the antinodal directions [55]. Including this effect would improve

the fits, since it would require a larger value of A. We therefore focus on the red lines and use the green curves to estimate an upper error bound. From the difference between the black curves and the red lines in Fig. 7 we see the effect of the CDW at 100 K for UD85 through to UD68 is approximately the same, for UD64 it is a factor of 2 smaller, while for UD62 and UD57 it is hardly detectable. We note that the deviations from the $T_c(p)$ parabolic law are still substantial for UD85 samples [35]. Therefore, bearing in mind our argument that the p values for UD57 and UD62 are essentially the same, we can conclude that all the data in Fig. 7 are consistent with the suggestions, previously formulated in terms of electronic phase separation [56] and stripe order [35,57,58], that the CDW actually causes the plateau in $T_c(x)$ by suppressing T_c below the parabolic law when p is between 0.11 and 0.14.

C. Numerical comparison with hard x-ray diffraction data for UD67

In order to estimate the magnitude of the changes expected in $d\chi_{ab}(T)/dT$ we use the published hard x-ray diffraction data of Chang *et al.* [8] for UD67 and make a comparison with our data for UD68 that has $T_c = 67.9$ K. Any CDW gap $\Delta_{CDW}(T)$ in the electronic DOS will be proportional to the amplitude of ionic displacements [27] that is to the square root of the intensity of the CDW diffraction peaks. In view of the competition between CDWs and superconductivity [8] it is reasonable to assume that $\Delta_{CDW}(0) \simeq 36$ meV, a typical value quoted for the maximum of the d-wave superconducting energy gap parameter in underdoped cuprates [59]. This normalization gives $\Delta_{CDW}(T)$ shown in Fig. 8.

We use a model in which there is a uniform CDW gap, of the same states-conserving form that also occurs in
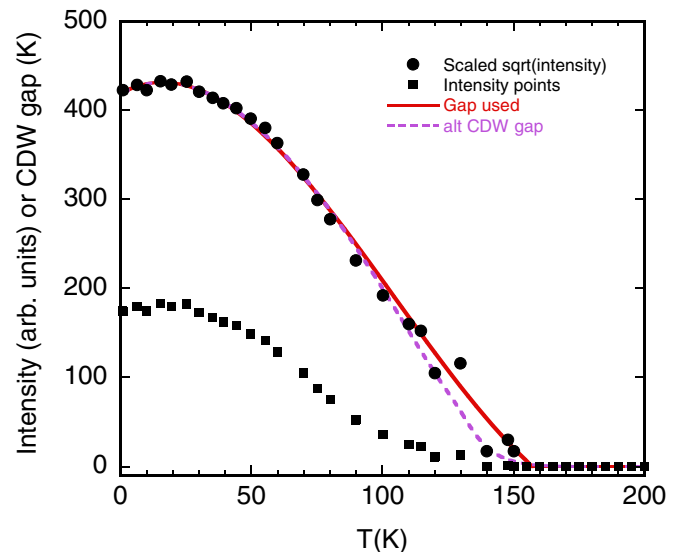

FIG. 8. Intensity (black squares) of CDW diffraction peak vs T for UD67 in an applied field of 17 T that severely weakens superconductivity, taken from Ref. [8] and the corresponding CDW energy gap (solid circles), assuming that it has a maximum value of 433 K or 37.3 meV. Note the relatively small values, $\Delta_{CDW}(T)/k_BT < 2$ above 100 K. The solid red curve shows the T-dependent CDW gap used in model calculations. The alternative dashed curve gives slightly smaller effects in $d\chi_{ab}(T)/dT$ just below T_{CDW}.
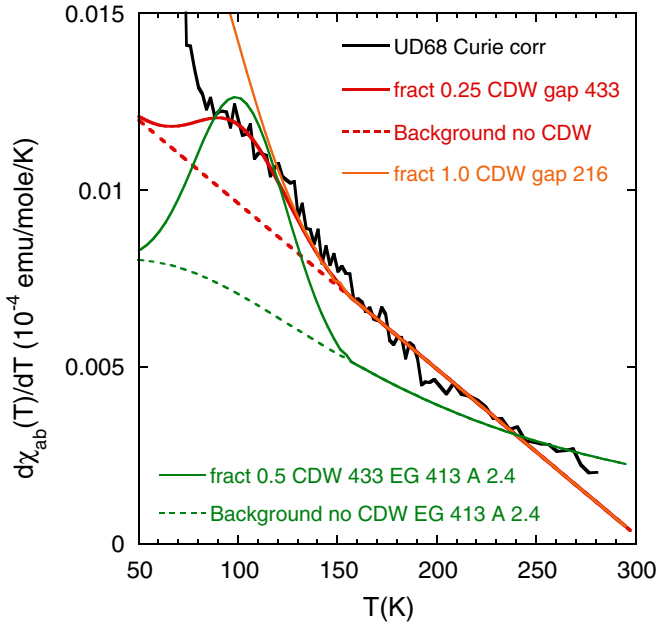
FIG. 9. Comparison of measured values of $d\chi_{ab}(T)/dT$ for UD68 ($T_c = 67.9$ K), with calculations using CDW energy gaps derived from the x-ray intensity shown in Fig. 8 and a simple Fermi arc, solid red curve, and pseudogap model, green curve (see text). The best agreement, shown by the solid red line, is given for a CDW gap rising to ~433 K at low T that reduces the lengths of the arcs by a factor ~0.75. Deviations from the solid red line below 80 K could arise from a reduction in electronic DOS caused by superconducting fluctuations. Green curves correspond to a background given by Eq. (1) with $A = 2.4 \times 10^{-4}$ emu/mol and $E_G/k_B = 413$ K. Values of the fitting parameter fract, the fractional length of the arcs affected by the CDW are also shown.

superconductivity, over a certain length of the Fermi arcs (specified by the parameter "fract" in Fig. 9) and then calculate $\chi_{ab}(T)$ and $d\chi_{ab}(T)/dT$ using standard expressions and Fermi statistics. It can be seen that the magnitude and T dependence of the effect are well described with $\Delta_{CDW}(0) = 433$ K and the CDW gap only extending over 25% of the length of the arcs, i.e., over only 5% of the circumference of the large quasi-two-dimensional Fermi surface present in overdoped cuprates. Even for such a large value of $\Delta_{CDW}(0)$, $\Delta_{CDW}(T)$ above 100 K is comparable with, or less than, $2k_BT$ so one would not expect to see effects associated with closed electron pockets on transport properties in low magnetic fields in this range of T. This provides support for the model involving electron-electron scattering between Fermi arcs proposed by Gor'kov [60] in connection with the T^2 dependence of the in-plane resistivity of UD HgBa$_2$CuO$_{4+x}$ [61].

On the other hand, there are indications of possible inconsistencies with other work that need further study. For a d-wave superconducting gap that rises to 433 K at the antinodes, then for arc lengths of 20% the gap at the ends of the arcs, will only be 433 sin(18) or 134 K which would not be large enough to suppress a CDW with a gap of 433 K. As shown in Fig. 9 a smaller value of $\Delta_{CDW}(0) = 216$ K does not give a good fit to the data. The parameter fract has to be 1.0 in order to account for the slope of the data between
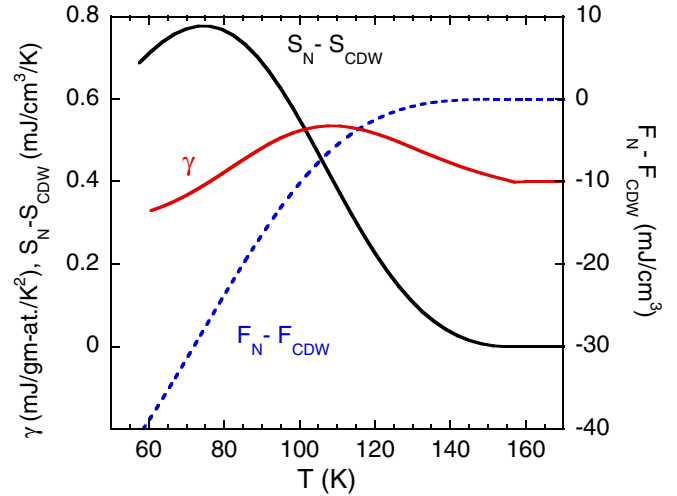

FIG. 10. Calculated changes in electronic entropy $S_N - S_{CDW}$ of UD68 caused by the onset of the CDW below $\simeq 150$ K. The contributions to S_N and S_{CDW} from the Fermi arcs were calculated using the same parameters that give a good fit to the data for UD68 in Fig. 9. The electronic heat capacity was then found from the thermodynamic relation ($\gamma = C_{el}/T = dS/dT$) and the difference in Helmholtz free energies $F_N - F_{CDW}$ from $F = -dS/dT$. Absolute magnitudes are obtained by normalizing to the experimental value for YBa$_2$Cu$_3$O$_7$ where there is no pseudogap, $\gamma = 2$ mJ/g at. K^{-2} [51].

120 and 150 K. and then this value of $\Delta_{CDW}(0)$ does not give such a good fit at lower T, as shown in Fig. 9. ARPES data for several cuprates (including Bi$_2$Sr$_2$CuO$_{6+\delta}$) shown in Fig. 10(b) of Ref. [14] give average arc lengths just above T_c rising from 23% to 27% between $p = 0.1$ and 0.125 which is reasonably consistent with our minimal model. For some unknown reason the arc length for Bi$_2$Sr$_2$CuO$_{6+\delta}$ at $p = 0.12$ shown in Ref. [9] is much larger (50%). We should also mention that in the Fermi arcs picture used here there is nothing particularly special about the doping level $p = 1/8$ where the suppression of T_c by the CDW reaches a maximum [35].

An alternative picture which would be in better agreement with scanning tunneling spectroscopy studies [62] would be to have longer arcs. In this case the arcs would need to have lower spectral weight in order to maintain the same superfluid density and the scenario in which the CDW wave vector connects the tips of the arcs would be less convincing. In this picture the detailed model is somewhat different but any CDW-induced anomalies in $d\chi_{ab}(T)/dT$ would still be small, because of the reduction in electronic DOS and entropy caused by the reduced spectral weight.

However, we are reluctant to abandon the concept of Fermi arcs because it could be very important for understanding the effect of a magnetic field on the CDW. The Lorentz force from a magnetic field perpendicular to the CuO$_2$ planes drives electrons from one end of the Fermi arc to the other. In a very simple qualitative picture this tends to pile up charge at one tip of an arc and to deplete it at the other, which would enhance a CDW in an applied magnetic field even when superconductivity has been heavily weakened or destroyed. There is experimental evidence in favor of this suggestion in

that the CDW intensity in UD67 increases strongly between 25 and 28 T [22].

D. Estimates of the changes in free energy associated with the CDW transitions

The small size of the CDW anomalies discussed in the previous section raises questions as to what is driving the CDW and how much free energy is gained by opening a CDW gap in the electronic DOS. We can answer the second question by continuing to model the data in terms of fermionic quasiparticles. Although this is the electronic contribution, in the harmonic approximation there is no change in the lattice entropy in the CDW state [63], so this a reasonable initial estimate. Despite the undoubted importance of electron-electron correlations, a fermion picture seems be relevant for hole-doped cuprates because their Wilson ratio is close to the value for weakly interacting fermions [46].

The entropy, specific heat, and free energy differences calculated in this model, with the same parameters used for the best fit in Fig. 9, are shown in Fig. 10. We see that at 100 K $F_N - F_{CDW} = 10$ mJ/cm^3 for UD68. Taking the average in-plane coherence length of the CDW, ξ_{CDW} to be 6 nm at 100 K [7], together with the c-axis spacing $d = 1.17$ nm gives the free energy difference multiplied by the appropriate coherence volume $\xi_{CDW}^2 d$ as only 30 K at 100 K and rising to ∼70 K at 80 K. This strongly suggests that thermal fluctuations are highly significant, in agreement with the suggestion in Ref. [4]. This estimate does depend on the method used to subtract the background contribution when making the fit to the UD68 data. As shown in Fig. 9 using a background based on Eq. (1), which does not give such a good fit, the effect of the CDW is approximately a factor 2 larger. There is also uncertainty arising from the possibility that T_{CDW} is significantly higher for our twinned UD68 sample than for the detwinned one studied in Ref. [8]. Together these two uncertainties could increase the effect of the CDW by up to a factor 3, but even then our estimate of $F_N - F_{CDW}$ will not exceed 30 mJ/cm^3 so the free energy in a coherence volume at 100 K is definitely less than $k_B T$ at 100 K.

As shown in Fig. 10, the smallest estimate of the change in free energy below T_{CDW} gives a broad peak in γ near 110 K that is calculated to be 0.14 mJ/g at. K^{-2}. This is about 8% of the electronic term for a UD67 sample near 110 K [51]. We expect there to be a T-dependent background caused by the pseudogap, but the effect might possibly be detectable using the ratio method [51]. Such an experiment should be attempted because in principle the heat capacity (and the thermal expansion) could give larger effects than what we predict from the magnetic susceptibility. For example, (a) from new Raman-active modes attributed to the CDW [54] or (b) because the onset of the CDW induces a change in the pseudogap energy. Possibility (b) could be important for understanding the driving force for CDW formation. Taking the viewpoint that the pseudogap does not conserve states [51] but instead causes a shift in spectral weight by energies of 1200 K or more away from the chemical potential, then changes in E_G could alter the electronic free energy significantly and therefore affect the heat capacity, without necessarily showing up in the magnetic susceptibility. However, we have no explanation as to how the

CDW could cause changes in E_G since in a simple picture it would only cause a symmetric spatial modulation about an average value. Also no heat capacity anomalies arising from CDWs were seen in heat capacity studies of polycrystalline YBCO samples [51].

IV. SUMMARY AND CONCLUSIONS

We have measured the anisotropic magnetic susceptibility of seven crystals of YBa$_2$Cu$_3$O$_{6+x}$ and used a special method for separating out the Curie term caused by a small concentration of localized spins that are induced by disorder on the Cu-O chains. We show that this term flattens out above 200 K for all samples and discuss two possible mechanisms for this unusual effect. By assuming that our crystals have the same CDW onset temperatures as those measured by resonant x-ray scattering, we can detect small effects in the magnetic susceptibility associated with the formation of charge density waves. These are stronger for samples on the $T_c(x)$ plateau, supporting scenarios in which the charge density waves are the main cause of the plateau. The effects are very small, which we ascribe, at least partly, to the pseudogap reducing the electronic entropy and density of states above T_{CDW}. For UD68 we have analyzed them using a minimal model involving a cylindrical Fermi surface and short Fermi arcs. This analysis shows that the CDW causes a reduction in electronic free energy in a coherence volume that is less than $k_B T$ at 100 K and comparable with, or up to a factor 2 larger than, $k_B T$ at 80 K. This is consistent with CDW being a bulk effect, i.e., not necessarily nucleated around defects [4,20], but with a slow onset that is probably caused by thermal fluctuations. The Wilson ratio for the cuprates is similar to that expected for weakly interacting fermions [46]. Therefore, comparable values for the electronic free energy would be obtained using a more realistic band structure and different arc lengths, because of the general relation between the measured magnetic susceptibility and the electronic heat capacity. Estimates of the size of the CDW gap suggest that there are unlikely to be significant CDW-induced changes in transport properties at 100 K at low magnetic fields, i.e., the Hall coefficient would be hole rather than electronlike in agreement with experimental data [15,48,57]. They also imply that, in the first approximation, all transport properties at low magnetic fields should be discussed in terms of Fermi arcs [60] rather than pockets of carriers. We have also put forward a qualitative explanation for the enhancement of the CDW by a large magnetic field. This involves a pile up of charge at the tips of the Fermi arcs that is induced by the Lorentz force. It remains to be seen whether this could be confirmed by calculating the magnetic field dependence of the Q-dependent charge susceptibility $\chi(Q)$ for Fermi arcs. One possible approach might be along the same lines as the calculations [64] of $\chi(Q)$ that account for field induced spin density waves in the quasi-one-dimensional Bechgaard salts.

---

[1] N. Doiron-Leyraud, C. Proust, D. LeBoeuf, J. Levallois, J.-B. Bonnemaison, R. Liang, D. A. Bonn, W. N. Hardy, and L. Taillefer, Nature (London) **447**, 565 (2007).

[2] E. A. Yelland, J. Singleton, C. H. Mielke, N. Harrison, F. F. Balakirev, B. Dabrowski, and J. R. Cooper, Phys. Rev. Lett. **100**, 047003 (2008).

[3] A. F. Bangura, J. D. Fletcher, A. Carrington, J. Levallois, M. Nardone, B. Vignolle, P. J. Heard, N. Doiron-Leyraud, D. LeBoeuf, L. Taillefer, S. Adachi, C. Proust, and N. E. Hussey, Phys. Rev. Lett. **100**, 047004 (2008).

[4] T. Wu, H. Mayaffre, S. Krämer, M. Horvatić, C. Berthier, W. N. Hardy, R. Liang, D. A. Bonn, and M.-H. Julien, Nat. Commun. **6**, 6438 (2015).

[5] G. Ghiringhelli *et al.*, Science **337**, 821 (2012).

[6] A. J. Achkar, R. Sutarto, X. Mao, F. He, A. Frano, S. Blanco-Canosa, M. Le Tacon, G. Ghiringhelli, L. Braicovich, M. Minola, M. Moretti Sala, C. Mazzoli, R. Liang, D. A. Bonn, W. N. Hardy, B. Keimer, G. A. Sawatzky, and D. G. Hawthorn, Phys. Rev. Lett. **109**, 167001 (2012).

[7] S. Blanco-Canosa, A. Frano, E. Schierle, J. Porras, T. Loew, M. Minola, M. Bluschke, E. Weschke, B. Keimer, and M. Le Tacon, Phys. Rev. B **90**, 054513 (2014).

[8] J. Chang, E. Blackburn, A. T. Holmes, N. B. Christensen, J. Larsen, J. Mesot, R. Liang, D. A. Bonn, W. N. Hardy, A. Watenphul, M. v. Zimmermann, E. M. Forgan, and S. M. Hayden, Nat. Phys. **8**, 871 (2012).

[9] R. Comin, A. Frano, M. M. Yee, Y. Yoshida, H. Eisaki, E. Schierle, E. Weschke, R. Sutarto, F. He, A. Soumyanarayanan, Y. He, M. Le Tacon, I. S. Elfimov, J. E. Hoffman, G. A. Sawatzky, B. Keimer, and A. Damascelli, Science **343**, 390 (2014).

[10] E. H. da Silva Neto, P. Aynajian, A. Frano, R. Comin, E. Schierle, E. Weschke, A. Gyenis, J. Wen, J. Schneeloch, Z. Xu, S. Ono, G. Gu, M. Le Tacon, and A. Yazdani, Science **343**, 393 (2014).

[11] M. Hücker, M. v. Zimmermann, G. D. Gu, Z. J. Xu, J. S. Wen, G. Xu, H. J. Kang, A. Zheludev, and J. M. Tranquada, Phys. Rev. B **83**, 104506 (2011).

[12] T. P. Croft, C. Lester, M. S. Senn, A. Bombardi, and S. M. Hayden, Phys. Rev. B **89**, 224513 (2014).

[13] E. Blackburn, J. Chang, M. Hücker, A. T. Holmes, N. B. Christensen, R. Liang, D. A. Bonn, W. N. Hardy, U. Rütt, O. Gutowski, M. v. Zimmermann, E. M. Forgan, and S. M. Hayden, Phys. Rev. Lett. **110**, 137004 (2013).

[14] T. Yoshida, M. Hashimoto, I. M. Vishik, Z.-X. Shen, and A. Fujimori, J. Phys. Soc. Jpn. **81**, 011006 (2012).

[15] D. LeBoeuf, N. Doiron-Leyraud, B. Vignolle, M. Sutherland, B. J. Ramshaw, J. Levallois, R. Daou, Francis Laliberté, Olivier Cyr-Choinière, J. Chang, Y. J. Jo, L. Balicas, R. Liang, D. A. Bonn, W. N. Hardy, C. Proust, and L. Taillefer, Phys. Rev. B **83**, 054506 (2011).

[16] B. Vignolle *et al.*, Nature (London) **455**, 952 (2008).

[17] T. Wu, H. Mayaffre, S. Krämer, M. Horvatić, C. Berthier, W. N. Hardy, R. Liang, D. A. Bonn, and M.-H. Julien, Nature (London) **477**, 191 (2011).

[18] T. Wu, H. Mayaffre, S. Krämer, M. Horvatić, C. Berthier, P. L. Kuhns, A. P. Reyes, R. Liang, W. N. Hardy, D. A. Bonn, and M.-H. Julien, Nat. Commun. **4**, 2113 (2013).

[19] L. Nie, G. Tarjus, and S. A. Kivelson, Proc. Natl. Acad. Sci. USA **111**, 7980 (2014).

[20] S. Blanco-Canosa, A. Frano, T. Loew, Y. Lu, J. Porras, G. Ghiringhelli, M. Minola, C. Mazzoli, L. Braicovich, E. Schierle, E. Weschke, M. Le Tacon, and B. Keimer, Phys. Rev. Lett. **110**, 187001 (2013).

[21] D. LeBoeuf, S. Krämer, W. N. Hardy, R. Liang, D. A. Bonn, and C. Proust, Nat. Phys. **9**, 79 (2013).

[22] S. Gerber, H. Jang, H. Nojiri, S. Matsuzawa, H. Yasumura, D. A. Bonn, R. Liang, W. N. Hardy, Z. Islam, A. Mehta, S. Song, M. Sikorski, D. Stefanescu, Y. Feng, S. A. Kivelson, T. P. Devereaux, Z. X. Shen, C. C. Kao, W. S. Lee, D. Zhu, and J. S. Lee, Science **350**, 949 (2015).

[23] J. Chang, E. Blackburn, O. Ivashko, A. T. Holmes, N. B. Christensen, M. Hücker, R. Liang, D. A. Bonn, W. N. Hardy, U. Rütt, M. v. Zimmermann, E. M. Forgan, and S. M. Hayden, Nat. Commun. **7**, 11494 (2016).

[24] E. M. Forgan, E. Blackburn, A. T. Holmes, A. Briffa, J. Chang, L. Bouchenoire, S. D. Brown, R. Liang, D. Bonn, W. N. Hardy, N. B. Christensen, M. v. Zimmermann, M. Hücker, and S. M. Hayden, arXiv:1504.01585.

[25] D. C. Johnston, Phys. Rev. Lett. **52**, 2049 (1984).

[26] J. R. Cooper, J. W. Loram, I. Kokanović, J. G. Storey, and J. L. Tallon, Phys. Rev. B **89**, 201104 (2014).

[27] G. Grüner, *Density Waves in Solids* (Addison Wesley, Reading, MA, 1994).

[28] I. Kokanović, J. R. Cooper, and K. Iida, Europhys. Lett. **98**, 57011 (2012).

[29] J. Biscaras, B. Leridon, D. Colson, A. Forget, and P. Monod, Phys. Rev. B **85**, 134517 (2012).

[30] R. S. Islam, J. R. Cooper, J. W. Loram, and S. H. Naqib, Phys. Rev. B **81**, 054511 (2010).

[31] Y. Shiohara and A. Endo, Mater. Sci. Eng. R **19**, 1 (1997).

[32] E. W. Ong, B. L. Ramakrishna, and Z. Iqbal, Solid State Commun. **66**, 171 (1988).

[33] Z. R. Wang, D. C. Johnston, L. L. Miller, and D. Vaknin, Phys. Rev. B **52**, 7384 (1995).

[34] X. G. Zheng, N. Tsutsumi, S. Tanaka, M. Suzuki, and C. N. Xu, Physica C **321**, 67 (1999).

[35] R. Liang, D. A. Bonn, and W. N. Hardy, Phys. Rev. B **73**, 180505 (2006).

[36] G. Xiao, M. Z. Cieplak, A. Gavrin, F. H. Streitz, A. Bakhshai, and C. L. Chien, Phys. Rev. Lett. **60**, 1446 (1988).

[37] M. v. Zimmermann, J. R. Schneider, T. Frello, N. H. Andersen, J. Madsen, M. Käll, H. F. Poulsen, R. Liang, P. Dosanjh, and W. N. Hardy, Phys. Rev. B **68**, 104515 (2003).

[38] UD85, 7 days in flowing air (A) at 540 °C, then 10 months at 25 °C (RT). UD77, 2.7 days A 555 °C, 30 months RT. UD72, 7 days A 570 °C, 2 months RT. UD68, 5 days A 590 °C, 2 months RT. UD64, 6 days A 610 °C, 1 month RT. UD62, 6 days A

640 °C, 10 months RT. UD57, 8 days flowing 1% O$_2$/N$_2$ 560 °C, 2 months RT.

[39] R. Liang, D. A. Bonn, and W. N. Hardy, Philos. Mag. **92**, 2563 (2012).

[40] B. J. Ramshaw, S. E. Sebastian, R. D. McDonald, James Day, B. S. Tan, Z. Zhu, J. B. Betts, R. Liang, D. A. Bonn, W. N. Hardy, and N. Harrison, Science **348**, 317 (2015).

[41] J. C. Baglo (private communication).

[42] A. J. Achkar, X. Mao, Christopher McMahon, R. Sutarto, F. He, R. Liang, D. A. Bonn, W. N. Hardy, and D. G. Hawthorn, Phys. Rev. Lett. **113**, 107002 (2014).

[43] A. K. R. Briffa, E. Blackburn, S. M. Hayden, E. A. Yelland, M. W. Long, and E. M. Forgan, Phys. Rev. B **93**, 094502 (2016).

[44] T. Watanabe, T. Fujii, and A. Matsuda, Phys. Rev. Lett. **84**, 5848 (2000).

[45] I. Kokanović, D. J. Hills, M. L. Sutherland, R. Liang, and J. R. Cooper, Phys. Rev. B **88**, 060505(R) (2013).

[46] J. R. Cooper and J. W. Loram, J. Phys. (France) I **6**, 2237 (1996).

[47] P. Nagel, V. Pasler, C. Meingast, A. I. Rykov, and S. Tajima, Phys. Rev. Lett. **85**, 2376 (2000).

[48] A. Carrington, D. J. C. Walker, A. P. Mackenzie, and J. R. Cooper, Phys. Rev. B **48**, 13051 (1993).

[49] H. Alloul, J. Bobroff, M. Gabay, and P. J. Hirschfeld, Rev. Mod. Phys. **81**, 45 (2009).

[50] A. Jánossy, L. C. Brünel, and J. R. Cooper, Phys. Rev. B **54**, 10186 (1996).

[51] J. W. Loram, J. Luo, J. R. Cooper, W. Y. Liang, and J. L. Tallon, J. Phys. Chem. Solids **62**, 59 (2001).

[52] D. E. Sheehy, T. P. Davis, and M. Franz, Phys. Rev. B **70**, 054510 (2004).

[53] T. Pereg-Barnea, P. J. Turner, R. Harris, G. K. Mullins, J. S. Bobowski, M. Raudsepp, R. Liang, D. A. Bonn, and W. N. Hardy, Phys. Rev. B **69**, 184513 (2004).

[54] M. Bakr, S. M. Souliou, S. Blanco-Canosa, I. Zegkinoglou, H. Gretarsson, J. Strempfer, T. Loew, C. T. Lin, R. Liang, D. A. Bonn, W. N. Hardy, B. Keimer, and M. Le Tacon, Phys. Rev. B **88**, 214517 (2013).

[55] M. Eschrig, Adv. Phys. **55**, 47 (2006).

[56] J. L. Tallon, G. V. M. Williams, N. E. Flower, and C. Bernhard, Physica C **282-287**, 236 (1997).

[57] K. Segawa and Y. Ando, J. Low Temp. Phys. **131**, 821 (2003).

[58] L. Taillefer, J. Phys.: Condens. Matter **21**, 164212 (2009).

[59] Ø. Fischer, M. Kugler, I. Maggio-Aprile, C. Berthod, and C. Renner, Rev. Mod. Phys. **79**, 353 (2007).

[60] L. P. Gor'kov, Phys. Rev. B **88**, 041104 (2013).

[61] N. Barišić, M. K. Chan, Y. Lie, G. Yua, X. Zhao, M. Dressel, A. Smontara, and M. Greven, Proc. Natl. Acad. Sci. USA **110**, 12235 (2013).

[62] Y. Kohsaka *et al.*, Nature (London) **454**, 1072 (2008).

[63] E. Tutiš (private communication).

[64] G. Montambaux, M. Héritier, and P. Lederer, Phys. Rev. Lett. **55**, 2078 (1985).